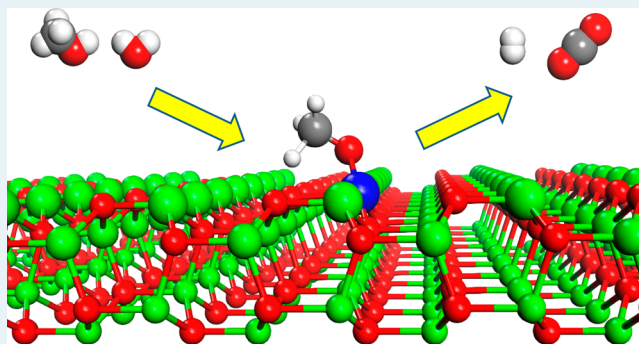


Supported Single Pt<sub>1</sub>/Au<sub>1</sub> Atoms for Methanol Steam ReformingXiang-Kui Gu,<sup>†,‡</sup> Botao Qiao,<sup>§,†,‡</sup> Chuan-Qi Huang,<sup>†</sup> Wu-Chen Ding,<sup>†</sup> Keju Sun,<sup>†</sup> Ensheng Zhan,<sup>§,†</sup> Tao Zhang,<sup>†</sup> Jingyue Liu,<sup>\*,§,†</sup> and Wei-Xue Li<sup>\*,†</sup><sup>†</sup>State Key Laboratory of Catalysis, Dalian Institute of Chemical Physics, Dalian National Laboratory for Clean Energy, Chinese Academic of Sciences, Dalian 116023, China<sup>§</sup>Department of Physics, Arizona State University, Tempe, Arizona 85287, United States

## Supporting Information

**ABSTRACT:** The single Pt<sub>1</sub> and Au<sub>1</sub> atoms stabilized by lattice oxygen on ZnO{10 $\bar{1}$ 0} surface for methanol steam reforming is reported. Density functional theory calculations reveal that the catalysis of the single precious metal atoms together with coordinated lattice oxygen stems from its stronger binding toward the intermediates, lowering reaction barriers, changing on the reaction pathway, enhancing greatly the activity. The measured turnover frequency of single Pt<sub>1</sub> sites was more than 1000 times higher than the pristine ZnO. The results provide valuable insights for the catalysis of the atomically dispersed precious metals on oxide supports.

**KEYWORDS:** single atom catalysis, methanol steam reforming, density functional theory, electron microscopy, activity, selectivity



In heterogeneous catalysis, metal particles are used to catalyze various industrially important chemical processes. To effectively utilize the desired, often expensive, precious metal, one usually disperses them onto high-surface-area supports with sizes ranging from a few nanometers down to subnanometers.<sup>1–4</sup> The presence of a large number of low-coordination sites on small particles is thought to be responsible for the enhanced catalytic activity.<sup>5</sup> To fully understand the structure–reactivity relationship of small particles or clusters, however, requires detailed knowledge of the active sites at the atomic level, which are often not available. Alternatively, metal species atomically dispersed onto oxide supports provide a well-defined system and have demonstrated excellent catalytic performance.<sup>6</sup> Moreover, such systems can provide a new platform to mimic homogeneous catalysis under heterogeneous environment.<sup>7,8</sup> Due to the recent advances of atomic resolution and in situ characterization techniques,<sup>9</sup> there is increasing interest in studying atomically dispersed catalysts. Furthermore, it is found that the active centers, responsible for the low-temperature activity of the water-gas-shift reaction<sup>10,11</sup> and CO oxidation,<sup>12,13</sup> can be attributed to the function of individual precious atoms strongly anchored onto the surfaces of oxide supports. Although the atomically dispersed catalysts may open a new and probably an efficient way to design novel classes of heterogeneous catalysts, it remains a challenge to fully uncover the nature of the active sites, to significantly improve their performance, and to develop strategies to prolong the stability of single-atom catalysts.

To address these questions, we report here a density functional theory (DFT) calculation, subangstrom resolution scanning transmission electron microscopy (STEM) character-

ization, and catalytic reactivity studies of single Pt<sub>1</sub> and Au<sub>1</sub> atoms dispersed onto ZnO nanowires (NWs) for methanol steam reforming (MSR).<sup>14–16</sup> The single Pt<sub>1</sub> and Au<sub>1</sub> atoms with atomic dispersion on ZnO was successfully prepared and identified to locate at the surface Zn lattice sites and stabilized by the lattice oxygen. Theoretical calculations show unambiguously that the single precious metal atoms together with coordinated oxygen bind more strongly toward the intermediates, improve the reaction energetics and kinetics, and change the reaction pathway. These eventually lead the single Pt<sub>1</sub> sites as the active sites with 1000 times higher turnover frequency (TOF) for MSR than that of the pristine ZnO.

ZnO NWs used in this work consist primarily of {10 $\bar{1}$ 0} facets (Figure S1a), and a loading of 0.0125 wt % of Au or Pt on ZnO NWs were prepared, as detailed in Supporting Information. Representative high-angle annular dark-field (HAADF) images of the Pt<sub>1</sub>/ZnO and Au<sub>1</sub>/ZnO catalysts are shown in Figure 1a,b, where the ZnO NWs were tilted with the electron beam close to [10 $\bar{1}$ 0] and [11 $\bar{2}$ 0] zone axis of ZnO (Figure S1b), respectively. The brighter dots represent single Pt and Au atoms (indicated by the yellow arrow) located on the Zn columns of the ZnO NW (denoted as Pt<sub>1</sub> and Au<sub>1</sub> hereafter). These isolated single atoms were relatively stable under electron beam irradiation, suggesting that they were anchored onto ZnO{10 $\bar{1}$ 0}. After analyses of many low- and high-magnification HAADF images (Figure S1c and d), we

Received: May 30, 2014

Revised: August 17, 2014

Published: September 29, 2014

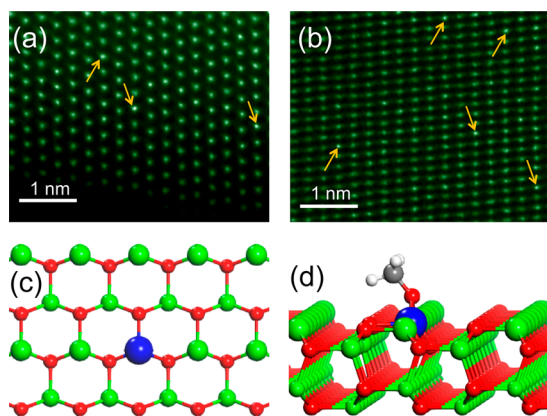


**Figure 1.** HAADF-STEM images of ZnO{1010} nanowires with embedded Pt<sub>1</sub> (a) and Au<sub>1</sub> (b) atoms (indicated by the yellow arrow), respectively. (c) Schematic structure for Pt<sub>1</sub>/Au<sub>1</sub>/ZnO{1010} (top view) and (d) Pt<sub>1</sub>/Au<sub>1</sub>/ZnO{1010} with adsorbed CH<sub>3</sub>O\* (side view). The blue, green, red, gray, and white spheres represent Pt<sub>1</sub>/Au<sub>1</sub>, Zn, O, C, and H atoms, respectively.

concluded that there were no Pt or Au clusters/particles in these Pt<sub>1</sub>/Au<sub>1</sub>/ZnO catalysts.

The stability of Pt<sub>1</sub>/Au<sub>1</sub>/ZnO can be explained if the observed single Pt<sub>1</sub> or Au<sub>1</sub> atoms are assumed to anchor onto the corresponding {1010} surface Zn vacancy positions (Figure 1c,d). DFT calculations showed that the corresponding formation energies of single Pt<sub>1</sub> and Au<sub>1</sub> atom are 0.22 and 0.86 eV lower than the reservoirs in equilibrium with infinite large metal counterparts, implying that the embedded Pt<sub>1</sub> and Au<sub>1</sub> are thermodynamically stable and resistant to segregation or agglomeration during the synthesis and/or the catalytic reactions. Pt<sub>1</sub> or Au<sub>1</sub> substituted at the subsurface Zn lattice sites would raise the corresponding energies by 0.45 and 0.70 eV and is energetically less favorable. On the other hand, the Pt<sub>1</sub> or Au<sub>1</sub> atoms positioned on top of the surface Zn sites is unstable and would displace to the bridge sites between Zn and O atoms at the grooves of ZnO{1010}, which was not observed. The stability of the Pt<sub>1</sub>/Au<sub>1</sub> sites originates from the strong chemical bonding between Pt<sub>1</sub>/Au<sub>1</sub> and the coordinated lattice oxygen, as seen from the extensive charge redistribution in Figure S2. Accordingly, Pt<sub>1</sub>/Au<sub>1</sub> atoms are in the cationic state.

The presence of surface embedded Pt<sub>1</sub>/Au<sub>1</sub> atoms changes dramatically the adsorption sites, their binding strength, and reaction energetics and barriers on the ZnO{1010} surface. The calculated binding energies for the reactants and intermediates involved in MSR at the most favorable site (Table S1 and Figure S3) are given in Figure 2. For CH<sub>3</sub>O\*, HCHO\*, HCO\*, CO\*, and OH\*, the corresponding binding strengths increase considerably by at least 0.99 eV on Pt<sub>1</sub>/ZnO, whereas at least 0.46 eV (maximum 1.84 eV) on Au<sub>1</sub>/ZnO. For H<sub>2</sub>O\* and CH<sub>3</sub>OH\*, the binding strengths increase only slightly, less than 0.15 eV in maximum on both Pt<sub>1</sub>/ZnO and Au<sub>1</sub>/ZnO. The presence of Pt<sub>1</sub> and Au<sub>1</sub> atoms also decrease the formation energies of the oxygen vacancy by at least 1.31 eV. This result agrees well with the previous calculations,<sup>17</sup> where the different valence of the substituted metal atoms from the host plays an essential role. These trends of variation in the binding energy are consistent with previous calculations.<sup>18</sup> The enhanced binding of the reactants/intermediates and decreased vacancy formation energy of oxygen due to the presence of Pt<sub>1</sub>/Au<sub>1</sub>

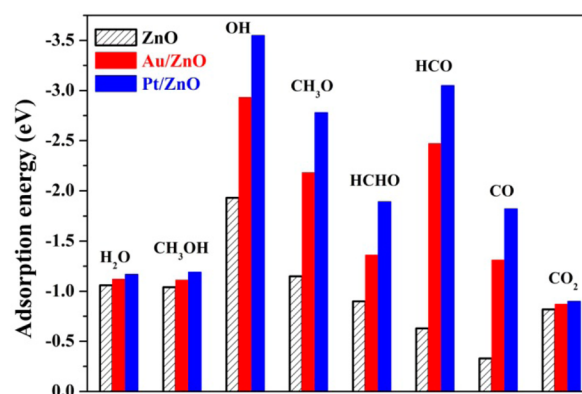


**Figure 2.** Calculated binding energies of the reactants and intermediates involved in MSR on ZnO{1010} (shadow), Au<sub>1</sub> (red solid), and Pt<sub>1</sub> (blue solid) embedded ZnO{1010}.

atoms improve reaction energetics and the subsequent reactivity, as detailed in below.

The significantly enhanced bonding of the reaction intermediates originates from their direct coordination to the Au<sub>1</sub>/Pt<sub>1</sub> atoms, as seen, for instance, from the CH<sub>3</sub>O\* adsorption structure in Figure 1d (additional detail in Figure S3). To reveal the electronic origin, the projected density of states (PDOS) is plotted in Figure S4. Compared to the Zn PDOS, there are considerable states available around the Fermi level for Pt<sub>1</sub> and Au<sub>1</sub>, which would make them more active. Moreover, the larger spatial extension of Pt<sub>1</sub> and Au<sub>1</sub> d-orbitals than that of Zn allows more extensive charge transfer and redistribution, as seen clearly from the charge density difference (Figure S5), forming a stronger chemical bond with the intermediates, accordingly.

The influence of the Pt<sub>1</sub>/Au<sub>1</sub> atoms on the dehydrogenation of H<sub>2</sub>O\* and CH<sub>3</sub>OH\* toward OH\*, CH<sub>3</sub>O\*, and CH<sub>2</sub>O\* (the initial elementary reaction steps in MSR) were calculated and plotted in Figure 3a (tabulated in Table S2). In terms of energetics, the sum of the binding energies of two reactants (H<sub>2</sub>O\* and CH<sub>3</sub>OH\*) on Pt<sub>1</sub>/ZnO is 0.26 eV lower than those on ZnO. Moreover, the reaction energetics  $\Delta E$  for the O–H bond scission of H<sub>2</sub>O\* and CH<sub>3</sub>OH\* are exothermic (–0.27

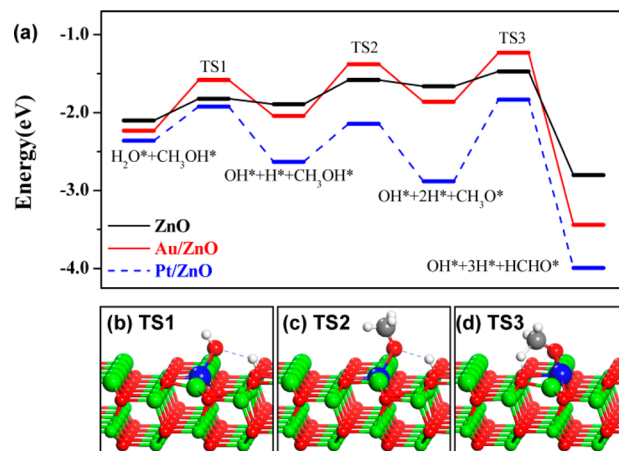


**Figure 3.** (a) Calculated potential energy surfaces for CH<sub>3</sub>OH\* + H<sub>2</sub>O\* → CH<sub>2</sub>O\* + OH\* + 2H\* on ZnO, Au<sub>1</sub>/ZnO, and Pt<sub>1</sub>/ZnO. (b), (c), and (d) are the schematic structures for the transition state TS1, TS2, and TS3 on Pt<sub>1</sub>/Au<sub>1</sub>/ZnO{1010}, respectively. The energy reference is gas phase H<sub>2</sub>O and CH<sub>3</sub>OH.

and  $-0.25$  eV) on  $\text{Pt}_1/\text{ZnO}$ , respectively, in contrast to the endothermic ( $0.21$  and  $0.23$  eV) on  $\text{ZnO}$ . For the subsequent C–H bond scission of  $\text{CH}_3\text{O}^*$  to  $\text{HCHO}^*$ , the difference of  $\Delta E$  between  $\text{Pt}_1/\text{ZnO}$  and  $\text{ZnO}$  is however negligible. The stronger binding of the reactants and favorable reaction energetics on  $\text{Pt}_1/\text{ZnO}$  than those on  $\text{ZnO}$  improve the overall energetics and therefore the corresponding reactivity. This has also been found for water dissociation on Pd-doped  $\text{ZnO}$ .<sup>19</sup> On the other hand, the calculated reaction barriers  $E_a$  for the above three reaction steps are  $0.44$ ,  $0.49$ , and  $1.05$  eV with the corresponding transition states TS1, TS2, and TS3 in Figure 3b, 3c, and 3d, respectively, which are all higher than those on  $\text{ZnO}$  ( $0.28$ ,  $0.31$ , and  $0.19$  eV). Such a behavior suggests that the overall potential energy surface (PES) becomes corrugated. Nevertheless, as seen from Figure 3a, the downshift of PES on  $\text{Pt}_1/\text{ZnO}$ , a consequence of the stronger binding of the reactants and improved  $\Delta E$  for the O–H bond scissions, is so significant that the corresponding TSs (blue bar) remains energetically lower than those of TSs (black bar) of  $\text{ZnO}$ . This implies that  $\text{Pt}_1/\text{ZnO}$  would have a higher reactivity than  $\text{ZnO}$ .

For  $\text{Au}_1/\text{ZnO}$ , the overall binding of two reactants enhances modestly by  $\sim 0.14$  eV compared to  $\text{ZnO}$ . Reaction energetics  $\Delta E$  in the subsequent O–H scissions remains endothermic ( $0.19$  and  $0.18$  eV), similar to those of  $\text{ZnO}$ . However, the corresponding O–H scission barriers  $E_a$  ( $0.65$  eV for  $\text{H}_2\text{O}^*$  and  $0.66$  eV for  $\text{CH}_3\text{OH}^*$ ) become even larger than those on  $\text{Pt}_1/\text{ZnO}$  ( $0.44$  and  $0.49$  eV). Namely, the  $\text{Au}_1/\text{ZnO}$  does not possess appreciable improvement in binding the reactants or the reaction energetics than those of  $\text{ZnO}$ , whereas the corresponding overall PES becomes more corrugated than that of  $\text{ZnO}$ . As a result, the values of the TSs (red bar in Figure 3a) are energetically even higher than those of  $\text{ZnO}$  (black bar).

The MSR experiments were carried out in a fixed-bed reactor with 50 mg of catalyst in about 60–80 mesh size. Pristine  $\text{ZnO}$ ,  $\text{Pt}_1/\text{ZnO}$ , and  $\text{Au}_1/\text{ZnO}$  NWs were tested. The products were  $\text{H}_2$ ,  $\text{CO}$ , and  $\text{CO}_2$  only within the detection limit, and the conversion was calculated based on the carbon balance. All three catalysts were very stable during the MSR reaction at  $390$  °C (Figure 4a). On the pristine  $\text{ZnO}$  NWs, the conversion was low ( $<10\%$ ), but the selectivity toward  $\text{CO}_2$  approached  $100\%$ , which agrees well with the recent literature reports.<sup>20,21</sup> The

$\text{Pt}_1/\text{ZnO}$  catalyst was much more active than that of the pristine  $\text{ZnO}$  with the corresponding conversion of about  $43\%$  at the steady state. The selectivity toward  $\text{CO}_2$  remained high, ca.  $88\%$ . The  $\text{Au}_1/\text{ZnO}$  catalyst was also much more active than the pristine  $\text{ZnO}$  NWs with a conversion of about  $28\%$  and nearly  $100\%$   $\text{CO}_2$  selectivity.

Taking into account the extremely low levels of Pt and Au loading (only about 125 ppm), the differences in TOF values between these single-atom catalysts and the pristine surfaces of  $\text{ZnO}$  (measured in a kinetically controlled regime with methanol conversion less than  $20\%$ ) will be huge. For the pristine  $\text{ZnO}$  NWs primarily exposing  $\{10\bar{1}0\}$  surfaces with a total surface area of  $\sim 10$   $\text{m}^2/\text{g}$ , the corresponding TOF for MSR was calculated by assuming that all the Zn sites in the topmost layer of the  $\text{ZnO}$  surface are active centers. The calculated TOF at  $380$  °C is  $1.8 \times 10^{-2}$   $\text{s}^{-1}$ . For the  $\text{Pt}_1/\text{ZnO}$  and  $\text{Au}_1/\text{ZnO}$  catalysts, after subtracting the contribution from the surface Zn sites of the  $\text{ZnO}$  NWs, the corresponding TOF solely from the embedded  $\text{Au}_1$  and  $\text{Pt}_1$  sites for MSR were estimated to be  $4.7$  and  $18.9$   $\text{s}^{-1}$ , respectively, about two and three orders of magnitude higher than that of  $\text{ZnO}$ .

The TOF at different  $T$  varying from  $340$  to  $420$  °C were measured. The corresponding Arrhenius plots are shown in Figure 4b, from which the apparent activation energies  $E_{\text{app}}$  and pre-exponential factors  $A_{\text{app}}$  can be extracted. The  $E_{\text{app}}$  from lower to higher values, are  $1.05$ ,  $2.32$ , and  $2.58$  eV for  $\text{Pt}_1/\text{ZnO}$ ,  $\text{ZnO}$ ,  $\text{Au}_1/\text{ZnO}$ , respectively, with the corresponding  $A_{\text{app}}$  of  $2.4 \times 10^9$ ,  $1.7 \times 10^{16}$ ,  $3.2 \times 10^{20}$   $\text{s}^{-1}$ . The remarkable different  $A_{\text{app}}$  could be rationalized by the so-called compensation effect with respect to the corresponding  $E_{\text{app}}$  of the Arrhenius law found from various activation processes.<sup>22</sup> Namely, when the apparent activation energy changes, so does the pre-exponential factor. Among three catalysts studied here,  $\text{Pt}_1/\text{ZnO}$  has the lowest  $E_{\text{app}}$  and the smallest  $A_{\text{app}}$ , whereas  $\text{Au}_1/\text{ZnO}$  has the highest  $E_{\text{app}}$  and the largest  $A_{\text{app}}$ . It is likely that the much lower  $E_{\text{app}}$  of the  $\text{Pt}_1/\text{ZnO}$  and higher  $A_{\text{app}}$  of the  $\text{Au}_1/\text{ZnO}$  explains their three and two orders of magnitude higher TOF than that of  $\text{ZnO}$ . We note that the MSR on  $\text{ZnO}$  powder catalysts has been studied and the measured  $E_{\text{app}}$  was found to be less than  $100$ – $200$  kJ/mol.<sup>20,21</sup> The smaller  $E_a$  may have originated from the contribution of surfaces other than the  $\{10\bar{1}0\}$  surfaces, for example, polar surfaces, or defect sites present in  $\text{ZnO}$  powder catalysts.

To rationalize further the experimental findings on the trend variation of the MSR activity and selectivity toward  $\text{CO}_2$  and gain more mechanistic insights, the complete PESs on  $\text{ZnO}$ ,  $\text{Au}_1/\text{ZnO}$ , and  $\text{Pt}_1/\text{ZnO}$  were explored thoroughly, and the most favorable reaction pathways are shown in Figure 5 (detailed energetics, barriers, and TSs in Table S2). The reaction pathway toward  $\text{CO}_2$  could be classified into two pathways: Path I, association of formaldehyde from methanol with hydroxyl from water, and Path II, decomposition of formaldehyde to  $\text{CO}$  followed by water gas shift (WGS) reaction.<sup>23</sup> The pathway via methyl formate was not considered here because it was found to be of minor importance.<sup>24</sup>

First of all, we note that among all of the optimized TSs, only the order of the relative height of TS3 and TS4 in the optimized PES ( $\text{Pt}_1/\text{ZnO} < \text{ZnO} < \text{Au}_1/\text{ZnO}$ ) follows the same order of the measured apparent activation energies. This indicates that either TS3 or TS4 could be the potential rate-determining state contributing to the measured apparent activation energy. Compared to TS4, the relative height of TS3 is higher, and would be more demanding to approach.

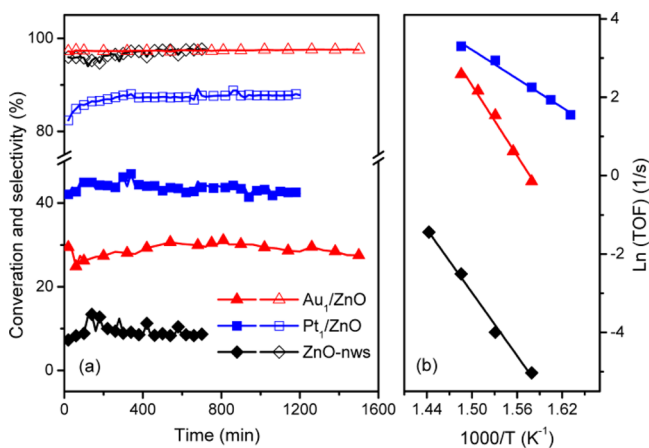


**Figure 4.** (a) Methanol conversion (solid) and  $\text{CO}_2$  selectivity (open) as a function of reaction time at  $390$  °C on  $\text{Au}_1/\text{ZnO}$  (red triangle),  $\text{Pt}_1/\text{ZnO}$  (blue square) catalysts, and the pristine  $\text{ZnO}$  nanowires (black diamond); (b) corresponding Arrhenius plots of the reaction rate  $\text{Ln}(\text{TOF})$  ( $\text{s}^{-1}$ ) versus  $1/T$  for the MSR reaction.



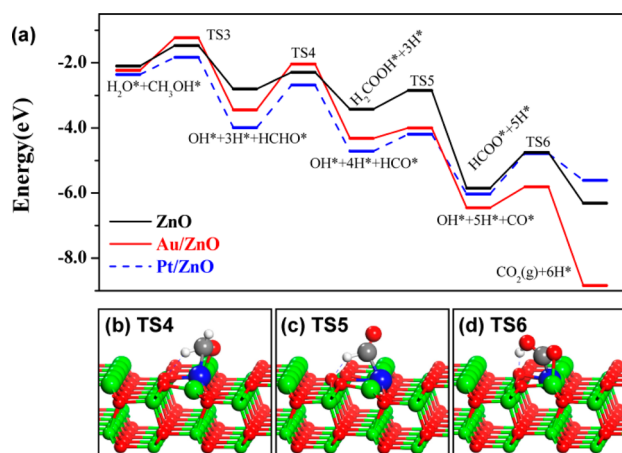


**Figure 5.** (a) Calculated most favorable reaction pathways for  $\text{CH}_3\text{OH}^* + \text{H}_2\text{O}^* \rightarrow \text{CO}_2 + 6\text{H}^*$  on ZnO,  $\text{Au}_1/\text{ZnO}$ , and  $\text{Pt}_1/\text{ZnO}$  without showing TS1 and TS2 explicitly. (b), (c) and (d) are the schematic structures for the transition state TS4, TS5, and TS6 on  $\text{Pt}_1/\text{Au}_1/\text{ZnO}\{10\bar{1}0\}$ , respectively. The energy reference is gas phase  $\text{H}_2\text{O}$  and  $\text{CH}_3\text{OH}$ .

Actually, TS3 represents the highest TS in the optimized PES, irrespective to the three catalysts studied. In the literature, the energetically highest transition state in the PES of a multistep reaction was suggested to be the rate-determining state closely related to the apparent activation energy.<sup>25</sup> Accordingly, we attribute attentively TS3 (the dehydrogenation of methoxy to formaldehyde) as the rate-determining step of MSR for the three catalysts considered here.

For  $\text{CO}_2$  selectivity on ZnO, the association of  $\text{CH}_2\text{O}^*$  with  $\text{OH}^*$  to form  $\text{H}_2\text{COOH}^*$  (Path I) has a modest reaction barrier  $E_a$  of 0.51 eV and exothermic reaction energetics of  $-0.62$  eV (TS4 in Figure S6). While for Path II, the dehydrogenation from  $\text{CH}_2\text{O}^*$  to  $\text{CHO}^*$  has a considerably high barrier  $E_a$  of 1.51 eV and endothermic reaction energetics  $\Delta E$  of 0.29 eV. Therefore, Path I is not only kinetically but also energetically more favorable than Path II. Once  $\text{H}_2\text{COOH}^*$  is formed, sequential dehydrogenation to  $\text{HCOO}^*$  and  $\text{CO}_2$  are exothermic with  $E_a$  of 0.57 and 1.10 eV (TS5 and TS6 in Figure S6), respectively. These results indicate that ZnO have a higher MSR selectivity toward  $\text{CO}_2$ , as evidenced by experiments.

On  $\text{Pt}_1/\text{ZnO}$  and  $\text{Au}_1/\text{ZnO}$ , because the overall binding energy of formaldehyde and hydroxyl is at least 1.46 eV stronger than those on ZnO, their association (Path I) becomes energetically less favorable, as seen from the change of reaction energetics from exothermic ( $-0.62$  eV for ZnO) to endothermic (larger than 0.65 eV). Kinetically, it also becomes less favorable because the corresponding barrier increases at least by 0.49 eV. On the other hand, the binding of formyl ( $\text{CHO}^*$ ) on  $\text{Pt}_1/\text{ZnO}$  and  $\text{Au}_1/\text{ZnO}$  is at least 1.83 eV stronger than that on ZnO. Therefore, the reaction energetics for dehydrogenation of  $\text{CH}_2\text{O}^*$  to  $\text{CHO}^*$  (Path II) would be improved. Indeed, the calculated reaction energetics changes from endothermic (0.29 eV for ZnO) to exothermic ( $-0.72$  eV at least), concurrently with a decrease of barrier by 0.20 eV for  $\text{Pt}_1/\text{ZnO}$  and 0.11 eV for  $\text{Au}_1/\text{ZnO}$  (TS4, Figure S6). The subsequent dehydrogenation of  $\text{CHO}^*$  to  $\text{CO}^*$  remains facile (TS5, Figure S6). These considerations suggest that on  $\text{Pt}_1/\text{ZnO}$  and  $\text{Au}_1/\text{ZnO}$  complete dehydrogenation of formaldehyde rather than its association with hydroxyl becomes favorable. To evaluate the overall processes of Path II, the WGS

reaction was studied. The calculated barriers of  $\text{CO}^*$  association with  $\text{OH}^*$  for  $\text{CO}_2$  are 1.24 and 0.64 eV for  $\text{Pt}_1/\text{ZnO}$  and  $\text{Au}_1/\text{ZnO}$ , respectively (TS6, Figure S6). The higher barrier for the previous one could be rationalized by the stronger binding of  $\text{CO}^*$  by 0.52 eV at  $\text{Pt}_1$  sites than  $\text{Au}_1$  sites, hindering energetically the formation of  $\text{CO}_2$ . This final step would result in a lower  $\text{CO}_2$  selectivity for  $\text{Pt}_1/\text{ZnO}$  than  $\text{Au}_1/\text{ZnO}$ , in agreement with experiment.

The calculations above show that although all the three catalysts have good selectivity toward  $\text{CO}_2$ , the corresponding reaction pathways are different when single atoms of  $\text{Pt}_1$  or  $\text{Au}_1$  are embedded onto the ZnO  $\{10\bar{1}0\}$  surfaces. Therefore, the  $\text{Pt}_1$  and  $\text{Au}_1$  do not act as promoters; together with the oxygen and Zn sites of ZnO, they form new active centers that are intrinsically different from the catalytic properties of ZnO.

In summary, isolated precious metal atoms including  $\text{Pt}_1$  and  $\text{Au}_1$  together with coordinated lattice oxygen embedded onto ZnO surfaces provide single yet stable active sites for methanol steam reforming. Such single active sites bind stronger toward the intermediates, have a more favorable reaction energetics and kinetics, and even change the reaction pathways. These lead to a great enhancement of the activity, and in particular, the single  $\text{Pt}_1$  sites embedded onto  $\text{ZnO}\{10\bar{1}0\}$  surfaces were found to have a TOF of over 1000 times higher than that of the pristine ZnO. The results in this study for the function of the surface-embedded single precious metal atoms on supports provide valuable insights for the catalysis of the single precious metal atoms embedded on the oxide surfaces.

## ■ ASSOCIATED CONTENT

### 📄 Supporting Information

Computational and experimental details, optimized reaction conditions and tests, calculated binding energies and reaction barriers, optimized structures and calculated charge density differences, and transition states for TS4, TS5, and TS6. This material is available free of charge via the Internet at <http://pubs.acs.org>.

## ■ AUTHOR INFORMATION

### Corresponding Authors

\*E-mail: [jingyue.Liu@asu.edu](mailto:jingyue.Liu@asu.edu).

\*E-mail: [wqli@dicp.ac.cn](mailto:wqli@dicp.ac.cn).

### Author Contributions

‡X.-K.G. and B.Q. contributed equally.

### Notes

The authors declare no competing financial interest.

## ■ ACKNOWLEDGMENTS

We are thankful for the financial support by the NSFC (nos. 21173210, 21103165, 21225315), 973 (no. 2013CB834603), and the start-up fund of the College of Liberal Arts and Sciences of Arizona State University (B.Q., E.Z., and J.L.). The authors also gratefully acknowledge the use of facilities in the John M. Cowley Center for High Resolution Electron Microscopy at Arizona State University, and calculations were carried out at the National Supercomputing Center “Tianhe-1” in Tianjin.

## ■ REFERENCES

- (1) Turner, M.; Golovko, V. B.; Vaughan, O. P. H.; Abdulkin, P.; Berenguer-Murcia, A.; Tikhov, M. S.; Johnson, B. F. G.; Lambert, R. M. *Nature* **2008**, *454*, 981–984.

- (2) Herzing, A. A.; Kiely, C. J.; Carley, A. F.; Landon, P.; Hutchings, G. J. *Science* **2008**, *321*, 1331–1335.
- (3) Judai, K.; Abbet, S.; Worz, A. S.; Heiz, U.; Henry, C. R. *J. Am. Chem. Soc.* **2004**, *126*, 2732–2737.
- (4) Lei, Y.; Mehmood, F.; Lee, S.; Greeley, J.; Lee, B.; Seifert, S.; Winans, R. E.; Elam, J. W.; Meyer, R. J.; Redfern, P. C.; Teschner, D.; Schlogl, R.; Pellin, M. J.; Curtiss, L. A.; Vajda, S. *Science* **2010**, *328*, 224–228.
- (5) Remediakis, I. N.; Lopez, N.; Norskov, J. K. *Angew. Chem., Int. Ed.* **2005**, *44*, 1824–1826.
- (6) Yang, X. F.; Wang, A. Q.; Qiao, B. T.; Li, J.; Liu, J. Y.; Zhang, T. *Acc. Chem. Res.* **2013**, *46*, 1740–1748.
- (7) Liu, Z. P.; Wang, C. M.; Fan, K. N. *Angew. Chem., Int. Ed.* **2006**, *45*, 6865–6868.
- (8) Motta, A.; Fragala, I. L.; Marks, T. J. *J. Am. Chem. Soc.* **2008**, *130*, 16533–16546.
- (9) Liu, J. Y. *ChemCatChem* **2011**, *3*, 934–948.
- (10) Zhai, Y. P.; Pierre, D.; Si, R.; Deng, W. L.; Ferrin, P.; Nilekar, A. U.; Peng, G. W.; Herron, J. A.; Bell, D. C.; Saltsburg, H.; Mavrikakis, M.; Flytzani-Stephanopoulos, M. *Science* **2010**, *329*, 1633–1636.
- (11) Lin, J.; Wang, A.; Qiao, B.; Liu, X.; Yang, X.; Wang, X.; Liang, J.; Li, J.; Liu, J.; Zhang, T. *J. Am. Chem. Soc.* **2013**, *135*, 15314–15317.
- (12) Qiao, B. T.; Wang, A. Q.; Yang, X. F.; Allard, L. F.; Jiang, Z.; Cui, Y. T.; Liu, J. Y.; Li, J.; Zhang, T. *Nat. Chem.* **2011**, *3*, 634–641.
- (13) Lin, J.; Qiao, B. T.; Liu, J. Y.; Huang, Y. Q.; Wang, A. Q.; Li, L.; Zhang, W. S.; Allard, L. F.; Wang, X. D.; Zhang, T. *Angew. Chem., Int. Ed.* **2012**, *51*, 2920–2924.
- (14) Palo, D. R.; Dagle, R. A.; Holladay, J. D. *Chem. Rev.* **2007**, *107*, 3992–4021.
- (15) Zhang, C.; Yuan, Z.; Liu, N.; Wang, S. *Fuel Cells* **2006**, *6*, 466–471.
- (16) Matsumura, Y.; Ishibe, H. *Appl. Catal., B* **2009**, *91*, 524–532.
- (17) McFarland, E. W.; Metiu, H. *Chem. Rev.* **2013**, *113*, 4391–4427.
- (18) Pala, R. G. S.; Metiu, H. *J. Catal.* **2008**, *254*, 325–331.
- (19) Gu, X. K.; Ding, W. C.; Huang, C. Q.; Li, W. X. *Chin. J. Catal.* **2012**, *33*, 1427–1431.
- (20) Lorenz, H.; Friedrich, M.; Armbruster, M.; Klotzer, B.; Penner, S. *J. Catal.* **2013**, *297*, 151–154.
- (21) Halevi, B.; Lin, S.; Roy, A.; Zhang, H.; Jeroro, E.; Vohs, J.; Wang, Y.; Guo, H.; Datye, A. K. *J. Phys. Chem. C* **2013**, *117*, 6493–6503.
- (22) Bligaard, T.; Honkala, K.; Logadottir, A.; Norskov, J. K.; Dahl, S.; Jacobsen, C. J. H. *J. Phys. Chem. B* **2003**, *107*, 9325–9331.
- (23) Gu, X. K.; Li, W. X. *J. Phys. Chem. C* **2010**, *114*, 21539–21547.
- (24) Lin, S.; Xie, D. Q.; Guo, H. *ACS Catal.* **2011**, *1*, 1263–1271.
- (25) Kozuch, S.; Shaik, S. *Acc. Chem. Res.* **2011**, *44*, 101–110.